

Token-Based Affordance Grounding with Large Vision-Language Models

Seung Il Lee¹, Qinqian Lei², Daguang Xu³, Dong Yang³,
Robby T. Tan², Yixin Chen¹, and Bo Wang¹

¹University of Mississippi · ²National University of Singapore · ³NVIDIA
<https://github.com/DrFirstLee/tokAG>

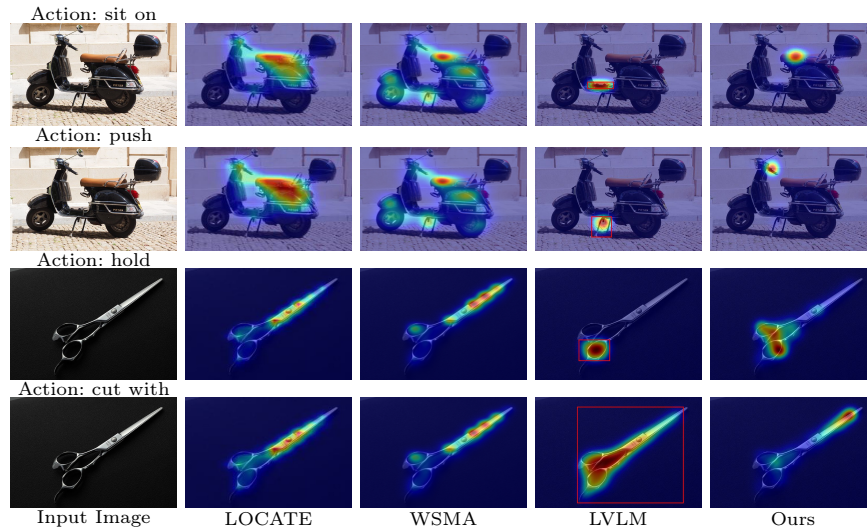


Fig. 1: Comparison of affordance grounding results. LOCATE [24] struggles with action co-occurrence in exocentric images, while WSMA [43] fails to distinguish semantically similar actions due to its reliance on short action phrases. Directly prompting a large vision-language model (LVLM, Qwen3-VL [3]) also produces inaccurate localization. Since LVLMs do not output heatmaps, the results are obtained using CLIPSeg [28]. In contrast, our method produces more accurate affordance localization.

Abstract. Affordance grounding aims to localize image regions that support a specific action, serving as a core capability for physical intelligence and embodied perception. Previous studies have primarily relied on weakly supervised learning with action labels from exocentric images. However, these methods often struggle with visually ambiguous exocentric images containing co-occurring actions; moreover, they fail to distinguish semantically similar actions because existing methods typically rely on brief action phrases that lack rich semantic details for action-specific localization. Although large vision-language models (LVLMs) encode rich action semantics and their action-conditioned textual outputs implicitly contain spatial cues, they do not directly provide action-specific spatial localization. To address these problems, we propose **TokAG**, a zero-shot

affordance grounding framework that exploits the token-level semantic-spatial signals in LVLMs to localize action-relevant regions without external supervision. We observe that attention maps associated with different LVM output tokens vary significantly, with many attending to irrelevant regions such as the background. Thus, we introduce a spatial-aware token-selection mechanism to systematically evaluate each output token and select the one whose attention maps exhibit dominant activation over the target object, instead of relying on arbitrary attention maps. By extracting these object-focused attention maps, we transform the LVM’s implicit semantic signals into zero-shot affordance heatmaps. Our zero-shot framework consistently outperforms prior weakly supervised approaches across multiple benchmarks, improving NSS by 10.7% on the unseen split of AGD20K and by 29.7% on HICO-IIF. The code and models will be made publicly available.

Keywords: Affordance Grounding · Vision-Language Models · Zero-Shot Learning

1 Introduction

The concept of affordance was introduced by Gibson [13] to describe action possibilities offered by the environment. In computer vision, affordance grounding aims to localize specific image regions that support potential human actions [29]. This task goes beyond object recognition, serving as a core capability for physical intelligence and embodied perception. Accurately understanding actionable regions is crucial for empowering a wide range of downstream applications, including robotic manipulation, human-computer interaction, and augmented reality, enabling artificial agents to navigate and interact with the 3D physical world safely [1, 2, 4, 14, 30, 45].

Despite recent progress, accurately grounding affordances remains challenging, especially in complex real-world scenarios where action understanding and spatial localization must work together. Previous studies primarily approach affordance grounding through weakly supervised learning, leveraging exocentric images with action-level supervision, where actions are typically represented as brief phrases. However, these methods [15, 24, 40] struggle with visually ambiguous exocentric images containing co-occurring actions. Our analysis shows that 31.7% of exocentric images are reused across different classes, capturing multiple actions (e.g., “brush with” and “hold” toothbrush) simultaneously. Such ambiguity prevents models from isolating action-specific visual evidence, leading to mislocalized predictions. As illustrated in the bottom two rows of Fig. 1, existing methods often produce identical heatmaps regardless of whether the action is “cut with” or “hold.”

Moreover, existing methods [33, 43, 44] fail to distinguish semantically similar actions on the same object. This limitation arises because they rely on brief action phrases that lack the semantic detail needed to disambiguate fine-grained actions and localize action-specific regions [21]. As shown in the first and second

rows of Fig. 1, existing methods struggle to differentiate nuanced actions such as “push” and “sit on” on the same motorcycle. While both actions involve the same object, they require grounding in distinct parts (the seat for sitting on and the handle for pushing), which existing methods often fail to isolate using weak action phrases alone.

Recently, large vision-language models (LVLMs) have demonstrated promising capabilities in visual understanding [3, 5, 22, 25, 42, 49]. These models encode rich action semantics, and their action-conditioned textual outputs implicitly contain spatial cues grounded in the visual input. However, LVLMs are primarily optimized for text generation rather than fine-grained, action-specific spatial localization [23]. Their internal attention mechanisms are not explicitly designed to produce precise affordance maps, making direct extraction of spatially accurate regions non-trivial.

Motivated by these observations, we propose **TokAG (Token-based Affordance Grounding)**, a zero-shot affordance grounding framework that leverages the cross-modal alignment between vision and language representations within LVLMs. Our approach directly localizes action-relevant regions without requiring external annotations or image-level supervision, enabling affordance grounding in a zero-shot setting. Importantly, our framework does not involve task-specific training or supervision for affordance localization. We observe that spatial activations within LVLMs vary substantially across output tokens, architectural layers, and attention heads, often exhibiting diffuse patterns that respond to irrelevant background context rather than target functional regions. This variability makes naive extraction of attention maps unreliable for affordance localization. Instead of relying on structural pruning [32] or layer and head selection strategies [18] that require supervision, we leverage the full cross-attention hierarchy of the LVLM and guide it using object-level spatial constraints. By aggregating activations across layers and heads, we preserve rich semantic-spatial cues while suppressing irrelevant background responses. Within this refined attention field, we identify the output token whose spatial activation is most concentrated on the target region. By isolating this token-specific activation map, we transform the LVLM’s implicit semantic knowledge into precise affordance heatmaps without any task-specific supervision. In summary, our main contributions are as follows:

- We introduce **TokAG**, a zero-shot affordance grounding framework that leverages latent semantic-spatial signals within pretrained LVLMs, eliminating the need for affordance-specific supervision.
- We propose a spatial-aware token-selection mechanism that aggregates cross-attention activations across layers and heads, and identifies object-focused tokens to produce precise affordance heatmaps.
- We provide an empirical analysis of the tokens selected by our framework, showing that they often correspond to action or object cues, and stronger LVLM backbones tend to select more semantically relevant tokens, which correlates with improved affordance grounding performance.

Notably, our zero-shot framework achieves an NSS of 1.514 on the unseen split of AGD20K, demonstrating a 10.7% improvement over the prior state-of-the-art

(1.368). Furthermore, on the HICO-IIF dataset, our method reaches an NSS of 1.655, representing a 29.7% increase compared to existing weakly supervised baselines (1.234).

2 Related Work

2.1 Weakly Supervised Affordance Grounding

Affordance grounding aims to localize object regions that support specific human actions [13]. Due to the high cost of obtaining pixel-level affordance, earlier works [9, 20, 35] primarily relied on fully supervised training, limiting scalability in complex real-world environments. To alleviate this issue, recent studies [11, 31, 36, 38] adopt weakly supervised learning paradigms that require only action-level supervision. These approaches can be broadly categorized into two groups based on their source of knowledge transfer.

Vision-Only Knowledge Transfer. The first line of research focuses on transferring visual knowledge from exocentric images with action-level supervision. Cross-View-AG [29] first introduced this paradigm by adopting the Class Activation Map (CAM) [48] mechanism to extract affordance cues from exocentric views in a weakly supervised manner. Subsequent methods have further improved this framework through more sophisticated transfer mechanisms. LOCATE [24] groups interaction embeddings from exocentric images into compact prototypes representing humans, object parts, and background regions to guide affordance grounding. INTRA [15] learns interaction representations directly from exocentric images, removing the need for paired datasets, while capturing unique interaction features through a contrastive learning framework. More recently, LoopTrans [40] introduces a closed-loop framework that enables bidirectional knowledge transfer between exocentric and egocentric views through a denoising knowledge distillation process. However, these approaches often struggle with visually ambiguous exocentric images containing multiple co-occurring actions, making it difficult to isolate action-specific affordance cues.

Vision-Language Knowledge Transfer. The second group incorporates textual information to improve affordance localization. WSMA [43] leverages both exocentric images and textual action labels to guide affordance localization in egocentric views through an HOI-Transfer module and a Pixel-Text Fusion module. It also introduces learnable prompts to refine the semantic representation of affordances. WSAG-PLSP [44] further explores this direction by employing large language models to refine affordance part descriptions and generate pseudo-labels using vision models such as VLPart [39] and SAM [19]. These pseudo-labels provide additional supervision during training. Meanwhile, Selective Contrastive Learning [33] utilizes CLIP [37] to transfer text-conditioned affordance knowledge across exocentric and egocentric views through selective contrastive objectives. Despite these advances, existing methods still rely on short action phrases, which often lack the rich semantic detail needed to distinguish semantically similar actions and accurately localize action-specific regions.

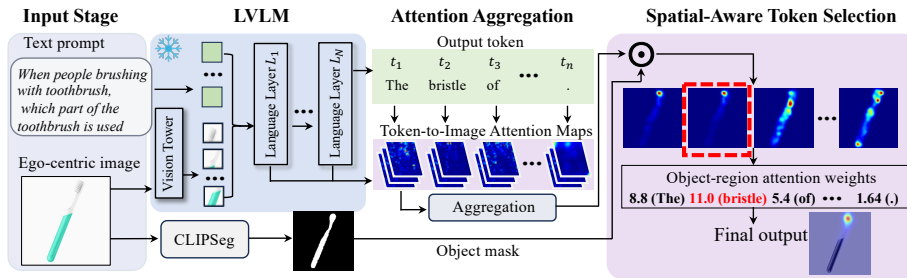


Fig. 2: Overview of the TokAG framework. Given an egocentric image and a text prompt, we extract output tokens (e.g., t_1, t_2, t_3) from the language layers of a frozen LVLm. We aggregate token-to-image attention maps across all layers and heads. With object masks generated by CLIPSeg [28], we compute object-region attention weights for each token. The token exhibiting the highest score is selected (e.g., t_2 , corresponding to “bristle” with a score of 11.0). The object-region attention heatmap corresponding to the selected token becomes the final prediction.

2.2 Visual Understanding and Localization in LVLms

Large Vision-Language Models (LVLms). Recent large vision-language models (LVLms), such as Qwen3-VL [3] and InternVL3 [49], have demonstrated promising progress in open-vocabulary visual understanding. These models achieve strong zero-shot performance on challenging multimodal benchmarks such as MMMU [46] and MathVista [27], which require reasoning beyond basic object recognition. Their ability to interpret complex visual scenes and generate descriptive textual outputs, such as identifying rare objects or explaining relationships within an image, highlights their strong semantic reasoning capabilities [3, 42, 49].

Localization Efforts in LVLms. Recent studies have explored training-free approaches for visual grounding by analyzing the internal states of multimodal large language models. Kang et al. [18] show that visual grounding can be achieved by leveraging a small subset of attention heads guided by the final token of the input prompt, while also identifying visual attention sinks that must be suppressed to improve localization accuracy [17]. Zhang et al. [47] further observe that LVLms may fail to explicitly describe small visual details. However, their internal attention patterns often correctly indicate where the model focuses its attention within the image. Based on this observation, they propose a training-free intervention strategy that uses attention and gradient maps to identify and crop relevant regions, improving the perception of small objects during inference. These studies suggest that the cross-modal attention mechanisms of LVLms encode useful spatial cues for visual localization. However, existing approaches utilize these attention signals to enhance text generation capabilities, or they rely on the heuristic selection of attention heads or tokens, which may not reliably isolate action-specific regions required for affordance grounding.

3 Method

We propose a zero-shot affordance grounding framework that localizes action-specific regions by extracting the implicit spatial knowledge of large vision-language models (LVLMs) without relying on external supervision. As illustrated in Fig. 2, our pipeline takes an egocentric image and a plain text prompt asking about the affordance area on a target object as inputs. Our method extracts and aggregates cross-modal attention maps utilizing a spatial-aware token selection mechanism to identify the most relevant action-conditioned spatial cues (Section 3.1). Furthermore, we observe that the selected tokens can often be decoded into meaningful semantic phrases of functional object parts, making our token selection mechanism interpretable (Section 3.2).

3.1 Attention Aggregation and Spatial-Aware Token Selection

Given an input image I , a target object O , and an action A , we formulate a simple text prompt P to query the LVLM: “*When people perform A with O , which part of the O is used for ‘ A ’? Answer in one sentence.*” Based on these input tokens, the LVLM generates a sequence of output tokens $T = \{t_1, t_2, \dots, t_N\}$. While LVLMs inherently encode rich action semantics, their textual responses do not provide explicit spatial coordinates. To bridge this gap, we analyze the cross-modal attention maps between generated output tokens and visual patches. As illustrated in Fig. 3, two key observations emerge. First, the spatial activations across layers and heads are diverse, often focusing on different image regions. Second, many attention responses are diffuse and may attend to task-irrelevant background regions due to the autoregressive generation process [17]. Meanwhile, we also observe that although the attention distributions vary across layers and heads, the activations that fall within the object region are typically related to the functional parts involved in the queried action. For example, when querying the action “sit on bed”, the model consistently highlights the mattress region. This behavior is intuitive because the attention maps originate from action-conditioned output tokens generated by the LVLM.

These observations motivate our spatial-aware token selection design. Instead of selecting specific layers or heads, we aggregate attention weights across all layers and attention heads to capture the distributed semantic-spatial cues within the LVLM. Formally, for each output token t_i , we obtain an aggregated attention map $\mathcal{M}_{t_i} \in \mathbb{R}^{H \times W}$ by integrating attention responses across the architectural layers and attention heads. Moreover, since attention activation inside the object region indicates useful affordance cues, we introduce an object-aware spatial constraint to suppress background noise and emphasize attention responses within the target object. To achieve this, we leverage a binary object mask $M_{obj} \in \{0, 1\}^{H \times W}$ for the target object O , generated by CLIPSeg [28].

First, we define the masked attention map $\widetilde{\mathcal{M}}_{t_i}$ by applying the object mask to the aggregated attention map via element-wise multiplication:

$$\widetilde{\mathcal{M}}_{t_i} = \mathcal{M}_{t_i} \odot M_{obj} \tag{1}$$

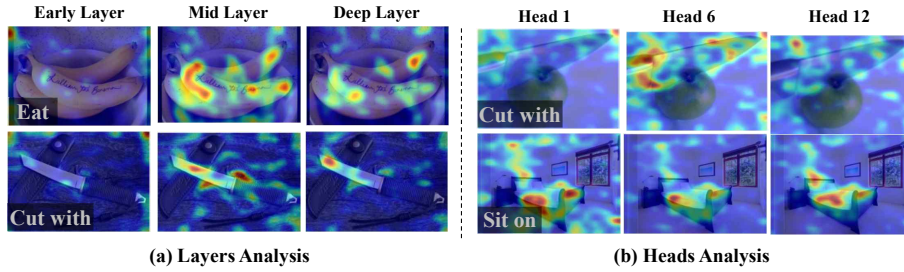


Fig. 3: Attention maps across various layers and heads. (a) Attention maps extracted from early, middle, and deep layers show different spatial activation patterns. (b) Different attention heads also focus on distinct image regions. These observations indicate that affordance-relevant cues are distributed across layers and heads, while some activations attend to task-irrelevant background regions.

where \odot denotes the Hadamard product. We then compute the overlap score S_i by aggregating the activation values of the masked attention map:

$$S_i = \sum_{x,y} \widetilde{\mathcal{M}}_{t_i}(x,y) \quad (2)$$

Then, we select the single output token t^* that yields the highest activation score over the target object area:

$$t^* = \underset{t_i \in T}{\operatorname{argmax}} S_i \quad (3)$$

Finally, the heatmap \mathcal{H} is derived by upsampling the selected masked attention map $\widetilde{\mathcal{M}}_{t^*}$ to the original image dimensions using bilinear interpolation: $\mathcal{H} = \operatorname{UP}(\widetilde{\mathcal{M}}_{t^*})$.

3.2 Analysis of Selected Tokens

Fig. 4 presents qualitative examples of the decoded texts corresponding to the output tokens selected by our spatial-aware token selection mechanism. Interestingly, many of these tokens correspond to meaningful object parts or functional regions, such as “blade”, “mattress”, “seat”, “handle”, and “cork”. These tokens naturally describe the regions that support the queried actions, suggesting that the LVLM implicitly encodes functional knowledge about objects.

To further analyze this phenomenon, we perform a semantic categorization of the selected tokens across the dataset, as summarized in Table 1. For the 2B model, approximately 55% of the selected tokens correspond to semantically meaningful action- or object-related words. This percentage increases to 65% when using the 32B model, suggesting that stronger semantic representations lead to more reliable token selection. This trend aligns with the improved affordance grounding performance observed with larger LVLM backbones.



Fig. 4: Examples of selected tokens. For each object–action pair, our spatial-aware token selection mechanism identifies the output token whose attention is most concentrated on the target object region. The selected token is then decoded into text for visualization. Interestingly, many decoded tokens correspond to meaningful object parts or functional regions (e.g., “blade”, “mattress”, “seat”, “handle”, and “cork”), which naturally align with the affordance-relevant areas.

Table 1: Semantic Analysis of Top-1 Tokens. Empirical results show that, the selected tokens correspond to meaningful affordance-related semantics. Specifically, 54.3% of the Top-1 tokens in the 2B model and 62.5% in the 32B model were identified as meaningful, indicating stronger semantic grounding with larger model sizes. The categories were initially assigned using GPT-based labeling and then verified by a human reviewer. The semantic categories are defined as follows: Meaningful Action (verbs such as ‘sit’ or ‘hold’), Object-Related Area (spatial terms like ‘top’, ‘bottom’, or ‘edge’), Function-Related (functional parts like ‘handle’, ‘seat’, or ‘blade’), and Others (grammatical articles like ‘a’ or ‘the’).

Model	Meaningful Action	Object-Related Area	Function-Related	Others
2B	23.0%	9.8%	21.5%	45.7%
32B	1.9%	20.2%	40.4%	37.6%

The key message is not that all the selected tokens are always meaningful, but that better models tend to select more meaningful tokens, and this correlates with better affordance localization. This gives us a more interpretable explanation of why the token-selection mechanism works and also suggests a possible direction for improving affordance grounding in the future.

4 Experiments

4.1 Experimental Setup

Datasets. We evaluate our method on two benchmark datasets for affordance grounding: AGD20K [29] and HICO-IIF [43]. AGD20K is a large-scale affordance grounding benchmark containing 20,061 exocentric images and 3,755 egocentric images annotated with 36 affordance categories. The dataset defines two evaluation settings based on action-object pair distributions. In the *Seen* setting, the training and test splits share identical action-object pairs (36 actions and 50 objects), differing only in the egocentric images used for evaluation. In the *Unseen* setting, the train and test splits share the same action categories but involve

Table 2: Performance comparison on the AGD20K dataset. Set 1 is the Seen test set, Set 2 is the Unseen test set. Lower is better for KLD (\downarrow), higher is better for SIM/NSS (\uparrow). The best performance is **bolded** and the second-best is underlined.

Method	AGD20K-Set 1			AGD20K-Set 2		
	KLD \downarrow	SIM \uparrow	NSS \uparrow	KLD \downarrow	SIM \uparrow	NSS \uparrow
Cross-View-AG (CVPR’22) [29]	1.538	0.334	0.927	1.787	0.285	0.829
Cross-View-AG+ (CVPR’22) [29]	1.489	0.342	0.981	1.765	0.279	0.882
LOCATE (CVPR’23) [24]	1.226	0.401	1.177	1.405	0.372	1.157
INTRA (ECCV’24) [15]	1.199	0.407	1.239	1.365	0.375	1.209
WSMA (AAAI’24) [43]	1.176	0.416	1.247	1.335	0.382	1.220
LoopTrans (ICCV’25) [40]	1.088	0.445	1.322	1.247	0.403	1.315
Moon et al. (ICCV’25) [33]	1.124	0.433	1.280	1.243	0.405	1.368
Ours (2B)	<u>1.020</u>	0.459	<u>1.406</u>	<u>1.060</u>	0.455	<u>1.514</u>
Ours (32B)	1.010	<u>0.458</u>	1.424	1.043	0.455	1.549

Table 3: Performance comparison on the HICO-IIF dataset (Seen test set). Lower is better for KLD (\downarrow), higher is better for SIM/NSS (\uparrow). The best performance is **bolded** and the second-best is underlined.

Method	KLD \downarrow	SIM \uparrow	NSS \uparrow
Cross-View-AG+ (CVPR’22) [29]	1.779	0.263	0.946
LOCATE (CVPR’23) [24]	1.593	0.327	0.966
WSMA (AAAI’24) [43]	1.465	0.358	1.012
LoopTrans (ICCV’25) [40]	1.399	0.379	1.226
Moon et al. (ICCV’25) [33]	1.358	0.378	1.234
Ours (2B)	<u>1.056</u>	0.459	<u>1.600</u>
Ours (32B)	1.032	<u>0.449</u>	1.655

non-overlapping object sets (e.g., training on “hold badminton racket” and testing on “hold axe”), which evaluates the model’s ability to generalize affordance understanding across different objects.

Existing weakly supervised methods [15, 24, 29, 33, 40, 43, 44] rely on transferring knowledge from exocentric training images and therefore explicitly train and evaluate under the *Seen* and *Unseen* settings. In contrast, our method operates in a zero-shot manner without using any training data from AGD20K. To avoid confusion with training-based protocols, we treat the two conventional evaluation settings as independent test splits, which we refer to as **Set 1** (Seen) and **Set 2** (Unseen). Apart from AGD20K dataset, HICO-IIF [43] is an affordance grounding benchmark derived from the HICO-DET dataset [7], containing human-object interaction images with pixel-level affordance annotations. Following existing methods [33, 40, 43], we evaluate our method on this dataset to assess generalization across different interaction scenarios and datasets.

Evaluation Metrics. Following standard evaluation protocols used in existing methods, we adopt three widely-used evaluation metrics to quantify the alignment between the predicted affordance heatmaps and the ground truth maps: Kullback-Leibler Divergence (*KLD*), Similarity (*SIM*), and Normalized Scan-path Saliency (*NSS*). Higher values for *SIM* and *NSS*, and lower values for *KLD*, indicate better grounding performance.

Implementation Details. Our method utilizes Qwen3-VL [3] as the LVLM to generate descriptive tokens and extract internal multi-head attention maps. For the spatial-aware token selection and the subsequent object-centric spatial alignment, we use the pre-trained CLIPSeg [28] model. All input images are uniformly resized to a spatial resolution of 1000×1000 pixels prior to processing. All experiments, including the LVLM inference and token-centric attention extraction, were conducted using an NVIDIA RTX 3090 GPU for the 2B model (an NVIDIA A100 GPU is used for the 32B model).

4.2 Comparison to State-of-the-art Methods

We compare our zero-shot framework against existing weakly-supervised affordance grounding methods [15, 24, 29, 33, 40, 43] on the AGD20K dataset (Table 2). Unlike these baselines, which rely on task-specific training on exocentric images, our approach operates in a zero-shot manner without using any training data. Our method demonstrates strong generalization to novel object categories (Set 2). As shown in Table 2, the **Ours** (2B) model achieves the lowest KLD (1.060) and the highest SIM (0.455) and NSS (1.514), outperforming previous best methods such as LoopTrans [40] (KLD: 1.247) and Moon et al. [33] (NSS: 1.368). These improvements highlight the ability of our framework to translate the implicit semantic knowledge of LVLMs into zero-shot affordance heatmaps.

Even on seen objects (Set 1), where baselines benefit from being trained on identical action-object pairs, our method remains competitive and achieves improved performance across all metrics. Specifically, the **Ours** (2B) model obtains the lowest KLD (1.020) and the highest SIM (0.459) and NSS (1.406). Finally, experiments with a larger backbone (32B) further improve performance across most metrics. To further evaluate the robustness and generalization ability of our framework, we also conduct experiments on the HICO-IIF dataset [43]. As summarized in Table 3, our method consistently outperforms all weakly-supervised baselines. In particular, the **Ours** (2B) model achieves the highest SIM (0.459) and NSS (1.600), while the larger **Ours** (32B) model further improves performance with the lowest KLD (1.032) and the highest NSS (1.655). These results demonstrate that our zero-shot framework generalizes well across datasets and interaction scenarios.

Runtime Evaluation. While TokAG delivers superior zero-shot performance, it entails higher computational cost due to the autoregressive inference of LVLM backbones. Specifically, TokAG operates at 0.59 FPS (2B) and 0.20 FPS (32B), whereas the weakly-supervised baseline WSMA [43] runs at 20.4 FPS. However, this inference overhead is reasonable because TokAG is training-free and does not require task-specific optimization.

Evaluation on Additional Dataset. We evaluate TokAG on EPIC-Aff [34], a challenging benchmark derived from EPIC-Kitchen [10]. We randomly sampled 500 images under the unseen condition, matching the scale of the AGD20K test set (540 images). On this dataset, TokAG outperforms WSMA across all metrics, achieving a lower KLD (3.367 vs. 3.372) and higher SIM (0.122 vs. 0.062) and NSS (0.927 vs. 0.413). As EPIC-Aff differs from object-centric affordance grounding benchmarks like AGD20K, EPIC-Aff contains less object-centric GT regions, which explains why the numbers are relatively low.

4.3 Evaluation of Foundation-Model-based Baselines

Although recent LVLMs demonstrate promising visual understanding capabilities, their standard textual outputs do not provide explicit spatial localization. Alternatively, vision foundation models (VFMs) such as SAM 3 [6] offer promising segmentation capabilities. To evaluate these alternative baselines with zero-shot capabilities, we compare TokAG with two groups of foundation-model-based baselines: (i) direct LVLm prompting methods for spatial coordinates, and (ii) multi-stage pipelines combining foundation models (e.g., LVLm + SAM 3 or GroundingDINO [26] + SAM 3). The results are summarized in Table 4.

Direct LVLm prompting performs poorly for affordance grounding. Using the same prompt as our framework, Method A (LVLm, Qwen3-VL [3]) produces only textual responses and therefore cannot generate spatial predictions. Method B follows the official grounding protocol of Qwen3-VL and prompts the model to predict bounding box coordinates, achieving an NSS of 1.085. Method C instead prompts the LVLm to output the center coordinate of the affordance region, resulting in worse performance (NSS 0.675, KLD 9.054).

Furthermore, combined foundation-model baselines (Methods D, E, and F) also show inferior performance compared to TokAG. Method D combines the predicted bounding box from the LVLm with a CLIPSeg segmentation mask via Hadamard product to obtain a pixel-level localization map. However, this refinement yields similar performance to Method B. While vision foundation models (VFMs) like SAM 3 excel at whole-object segmentation, they struggle to localize fine-grained functional regions, which is crucial for accurate affordance grounding. Consequently, these combined foundation-model baselines are less effective at capturing precise interaction regions, yielding inferior results (e.g., NSS of 1.189 and 0.657, respectively). Overall, these results indicate that although current foundation models capture rich semantic knowledge and object-level visual information, naively prompting LVLms or directly combining existing foundation models is insufficient to localize precise interaction regions for affordance grounding in a zero-shot setting. In contrast, TokAG bypasses explicit coordinate prediction and instead extracts spatial signals directly from cross-modal attention maps, enabling accurate affordance localization.

Additionally, TokAG doesn’t depend on the specific segmentation model. To demonstrate this flexibility, we test our model by using SAM3 instead of CLIPSeg. While the baseline by Moon et al. achieves an NSS of 1.368, our framework with SAM3 obtains an NSS of 1.416. Although this is slightly lower than

Table 4: Comparison with direct LVLm prompting and combined foundation-model baselines on the AGD20K Unseen (Set 2) dataset. (A) LVLm textual response; (B) Bounding box prediction from LVLm; (C) Gaussian-blurred anchor points from LVLm coordinate predictions; (D) Hadamard product of the predicted bounding box from LVLm and CLIPSeg mask; (E) Method B for bounding box prediction followed by segmentation with SAM 3; (F) Extracting object bounding boxes via Grounding-DINO followed by segmentation with SAM 3.

ID	Method	KLD ↓	SIM ↑	NSS ↑
A	LVLm ¹	Not available (Output was plain text)		
B	LVLm Bbox ²	5.336	0.347	1.085
C	LVLm Coord. ³	9.054	0.170	0.675
D	B + CLIPseg ⁴	5.684	0.346	1.085
E	B + SAM 3	3.229	0.438	1.189
F	[26] + SAM 3	3.110	0.319	0.657
G	TokAG (Ours)	1.060	0.455	1.514

¹Prompt: “Which part of [object] is used for [action]?”

²Add to prompt: “Output the bounding box of this part in [xmin, ymin, xmax, ymax] format. Scale coordinates from 0 to 1000.”

³Add to prompt: “Output the single center point coordinate in [x, y] format. Scale coordinates from 0 to 1000.” The predicted point is converted to a heatmap using Gaussian blurring for evaluation.

⁴CLIPSeg predicts a segmentation mask, which is combined with the LVLm bounding box via Hadamard product to obtain the final localization heatmap.

our default configuration with CLIPSeg (NSS 1.514), both variants consistently outperform the state-of-the-art.

To further analyze the impact of segmentation quality, we evaluated TokAG on 40 complex multi-object scenes, comparing cases with successful versus failed CLIPSeg outcomes. Successful segmentations yield an NSS of 1.665, whereas failures degrade performance to an NSS of 1.168. To investigate these limitations, we also conducted an error analysis on the AGD20K Unseen (Set 2) dataset, identifying 77 failure cases out of 540 test images. Among these, CLIPSeg segmentation errors account for 37.7% (29 cases), while token selection errors account for 62.3% (48 cases). This distribution indicates that while a reasonable object mask enhances performance, the primary remaining challenge lies in selecting semantically relevant tokens. Nevertheless, even under segmentation failure or when utilizing alternative architectures like SAM3, TokAG maintains competitive performance, verifying that our framework is not tied to a specific segmentation model.

Table 5: Evaluation of layer and head aggregation strategies on the AGD20K dataset (Set 2). Methods A–B evaluate different layer or head selections, while Method C aggregates attention across all layers and heads (ours).

	Type	Name	KLD ↓	SIM ↑	NSS ↑
(A-1)		L25-H5	1.132	0.441	1.431
(A-2)		L25	1.090	0.450	1.471
(A-3)	Layer & Head	H5	1.062	0.454	1.510
(B-1)	Selection	L16-H15	1.135	0.446	1.459
(B-2)		L16	1.100	0.461	1.466
(B-3)		H15	1.100	0.450	1.476
(C)		Ours	1.060	0.455	1.514

Table 6: Evaluation of token selection strategies for affordance grounding on the AGD20K dataset (Set 2). Methods D–H evaluate several heuristic token choices, while Method I corresponds to our spatial-aware Top-1 token selection.

	Type	Name	KLD ↓	SIM ↑	NSS ↑
(D)		Average All Tokens	1.111	0.435	1.457
(E)		First Output Token	1.078	0.444	1.493
(F)	Token	Last Output Token	1.358	0.364	1.116
(G)	Selection	Noun Tokens Only	1.112	0.435	1.461
(H)		Top-5 Tokens	1.084	0.444	1.482
(I)		Ours	1.060	0.455	1.514

4.4 Evaluation of the Token Selection Mechanism

Our framework converts the semantic knowledge of LVLMs into spatial affordance heatmaps through two key operations: (i) **layer/head aggregation** and (ii) **spatial-aware token selection**. We evaluate several alternative strategies for both components, with results summarized in Table 5 and Table 6.

Layer and Head Aggregation. Transformer models exhibit hierarchical representations where early layers encode spatial features while deeper layers capture semantic information [12]. Prior works in visual grounding often rely on selecting specific layers or attention heads (e.g., middle layers) to extract spatial signals [18]. However, identifying optimal layers or heads typically requires supervision or structural pruning [32], which is infeasible in our zero-shot setting.

We therefore compare several layer/head selection strategies (Table 5, A–B). Empirically, restricting attention extraction to individual layers or heads leads to inferior performance. In contrast, aggregating attention weights across all layers and heads (Method C) yields improved results (e.g., NSS 1.514). This suggests that affordance localization relies on distributed semantic-spatial cues across different layers and heads.

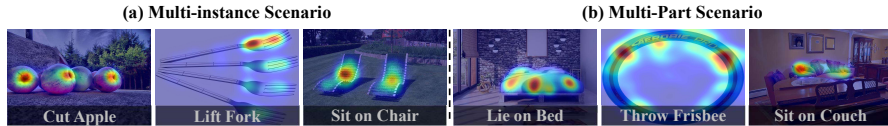


Fig. 5: Examples of Multi-objects and Multi-part scenarios

Token Selection Strategy. Existing visual grounding approaches typically rely on a predefined token, such as the [CLS] token in vision transformers [8, 41]. However, generative LVLMs do not contain a dedicated classification token, and therefore require alternative strategies. Previous work has explored using the first output token [47] or the last prompt token [18] for localization. To identify the most informative token for affordance grounding, we compare several token-selection strategies (Table 6, D–H), including: averaging all tokens, selecting the first output token, selecting the last output token, restricting to noun tokens, and selecting the Top- k tokens.

These strategies perform suboptimally in general. Averaging all tokens (Method D) introduces noise from non-informative tokens and results in spatially diffused attention maps. Similarly, relying on fixed positional tokens (Method E or Method F) degrades performance because these tokens often lack explicit semantic cues related to the affordance region.

Interestingly, restricting the selection to noun tokens (Method G) also underperforms. We observe that affordance-related activations frequently appear in articles (e.g., “a”, “the”) that precede the target noun. For example, in the phrase “cut with a knife,” the token “a” often produces the strongest spatial activation. This occurs because autoregressive attention for the current token is influenced by visual features required to predict the subsequent token, causing functional regions to be activated earlier in the generation process.

Finally, selecting multiple tokens (Top-5, Method H) slightly increases SIM due to broader spatial coverage, but degrades KLD and NSS as attention spreads beyond the primary functional region. In contrast, our spatial-aware Top-1 token selection (Method I) instead identifies the single token whose attention map shows the strongest activation over the target object. This mechanism effectively suppresses noise and autoregressive token drift, achieving the best overall performance (KLD 1.060, SIM 0.455, NSS 1.514).

Analysis of Multi-Instance and Multi-Part Scenarios. Although our token-selection strategy selects a single Top-1 token, the resulting localization is not restricted to a single spatial region as in Fig. 5. The cross-modal attention map of the selected token naturally captures multiple instances or functional parts, provided they share identical affordance properties. Consequently, TokAG can localize multi-instance and multi-part scenarios.

4.5 Failure cases

Fig. 6 shows representative failure cases where the predicted affordance heatmaps deviate from the true functional regions. These failures typically occur when the



Fig. 6: Representative failure cases of TokAG. In these examples, the predicted affordance heatmaps attend to incorrect or diffuse regions rather than the true functional parts. Such errors often occur when the affordance region is small, visually ambiguous, or attention mechanism is distracted by salient visual artifacts such as logos, text, or high-contrast markings on the object surface (e.g., the “REMO” logo on the drum).

target affordance region is small, visually ambiguous, or partially occluded, or when salient visual artifacts (e.g., logos or text) distract the attention mechanism from the true functional regions.

4.6 Limitations and Future Directions

Although TokAG performs well on existing benchmarks, it currently assumes that the target affordance can be represented by a single semantic token. This assumption aligns well with the object-centric affordance definitions used in current benchmarks, but may be insufficient for compositional affordances (e.g., “pour from” requiring both the handle and the spout) and bimanual interactions (e.g., opening a jar with one hand holding the jar and the other twisting the lid) that require simultaneous grounding of multiple functional regions. Developing multi-region reasoning and token aggregation strategies for compositional affordances is an important direction for future work.

5 Conclusion

We introduced **TokAG**, a novel zero-shot framework for affordance grounding that enables action-specific localization without requiring external supervision. TokAG leverages token-level semantic-spatial signals within large vision-language models (LVLMs) to transform their implicit action semantics into pixel-level affordance heatmaps. Our analysis shows that the spatial activations of LVLM output tokens contain meaningful cues for affordance localization. Rather than relying on noisy or arbitrary attention maps, TokAG employs a spatial-aware token selection mechanism that systematically identifies the output token whose attention map exhibits the strongest activation over the target object. Extensive experiments demonstrate that TokAG significantly improves affordance grounding performance. In particular, it improves the NSS metric by **10.7%** on the unseen split of AGD20K and by **29.7%** on HICO-IIF, consistently outperforming prior weakly supervised approaches and establishing a new state-of-the-art for zero-shot affordance grounding.

Acknowledgements. We thank the anonymous reviewers and area chairs for their constructive feedback, which helped improve this paper.

References

1. Ardón, P., Pairet, È., Lohan, K.S., Ramamoorthy, S., Petrick, R.: Affordances in robotic tasks—a survey. arXiv preprint arXiv:2004.07400 (2020)
2. Bahl, S., Mendonca, R., Chen, L., Jain, U., Pathak, D.: Affordances from human videos as a versatile representation for robotics. In: Proceedings of the IEEE/CVF Conference on Computer Vision and Pattern Recognition. pp. 13778–13790 (2023)
3. Bai, S., Cai, Y., Chen, R., Chen, K., Chen, X., Cheng, Z., Deng, L., Ding, W., Gao, C., Ge, C., et al.: Qwen3-vl technical report. arXiv preprint arXiv:2511.21631 (2025)
4. Brohan, A., Chebotar, Y., Finn, C., Hausman, K., Herzog, A., Ho, D., Ibarz, J., Irpan, A., Jang, E., Julian, R., et al.: Do as i can, not as i say: Grounding language in robotic affordances. In: Conference on robot learning. pp. 287–318. PMLR (2023)
5. Cao, X., Qu, Y., Xiao, W., Hu, J., Li, H., Liu, J., Huang, Z., Li, X., et al.: Smart-insertion-v: Photorealistic video insertion via a closed-loop feedback dual-stream framework. arXiv preprint arXiv:2605.23891 (2026)
6. Carion, N., Gustafson, L., Hu, Y.T., Debnath, S., Hu, R., Suris, D., Ryali, C., Alwala, K.V., Khedr, H., Huang, A., Lei, J., Ma, T., Guo, B., Kalla, A., Marks, M., Greer, J., Wang, M., Sun, P., Rädle, R., Afouras, T., Mavrouti, E., Xu, K., Wu, T.H., Zhou, Y., Momeni, L., Hazra, R., Ding, S., Vaze, S., Porcher, F., Li, F., Li, S., Kamath, A., Cheng, H.K., Dollár, P., Ravi, N., Saenko, K., Zhang, P., Feichtenhofer, C.: Sam 3: Segment anything with concepts (2025)
7. Chao, Y.W., Liu, Y., Liu, X., Zeng, H., Deng, J.: Learning to detect human-object interactions. In: 2018 IEEE winter conference on applications of computer vision (wacv). pp. 381–389. IEEE (2018)
8. Chefer, H., Gur, S., Wolf, L.: Transformer interpretability beyond attention visualization. In: Proceedings of the IEEE/CVF conference on computer vision and pattern recognition. pp. 782–791 (2021)
9. Chuang, C.Y., Li, J., Torralba, A., Fidler, S.: Learning to act properly: Predicting and explaining affordances from images. In: Proceedings of the IEEE Conference on Computer Vision and Pattern Recognition. pp. 975–983 (2018)
10. Damen, D., Doughty, H., Farinella, G.M., Fidler, S., Furnari, A., Kazakos, E., Moltisanti, D., Munro, J., Perrett, T., Price, W., et al.: The epic-kitchens dataset: Collection, challenges and baselines. *IEEE Transactions on Pattern Analysis and Machine Intelligence* **43**(11), 4125–4141 (2020)
11. Gao, W., Wan, F., Pan, X., Peng, Z., Tian, Q., Han, Z., Zhou, B., Ye, Q.: Ts-cam: Token semantic coupled attention map for weakly supervised object localization. In: Proceedings of the IEEE/CVF international conference on computer vision. pp. 2886–2895 (2021)
12. Ghiasi, A., Kazemi, H., Borgnia, E., Reich, S., Shu, M., Goldblum, M., Wilson, A.G., Goldstein, T.: What do vision transformers learn? a visual exploration. arXiv preprint arXiv:2212.06727 (2022)
13. Gibson, J.J.: The ecological approach to visual perception: classic edition. Psychology press (2014)
14. Hassanin, M., Khan, S., Tahtali, M.: Visual affordance and function understanding: A survey. *ACM Computing Surveys (CSUR)* **54**(3), 1–35 (2021)
15. Jang, J.H., Seo, H., Chun, S.Y.: Intra: Interaction relationship-aware weakly supervised affordance grounding. In: European Conference on Computer Vision. pp. 18–34. Springer (2024)

16. Jiang, M., Ruan, Y., Huang, S., Liao, S., Pitis, S., Grosse, R.B., Ba, J.: Calibrating language models via augmented prompt ensembles (2023)
17. Kang, S., Kim, J., Kim, J., Hwang, S.J.: See what you are told: Visual attention sink in large multimodal models. In: The Thirteenth International Conference on Learning Representations (2025)
18. Kang, S., Kim, J., Kim, J., Hwang, S.J.: Your large vision-language model only needs a few attention heads for visual grounding. In: Proceedings of the Computer Vision and Pattern Recognition Conference. pp. 9339–9350 (2025)
19. Kirillov, A., Mintun, E., Ravi, N., Mao, H., Rolland, C., Gustafson, L., Xiao, T., Whitehead, S., Berg, A.C., Lo, W.Y., et al.: Segment anything. In: Proceedings of the IEEE/CVF international conference on computer vision. pp. 4015–4026 (2023)
20. Koppula, H.S., Gupta, R., Saxena, A.: Learning human activities and object affordances from rgb-d videos. *The International journal of robotics research* **32**(8), 951–970 (2013)
21. Lei, Q., Wang, B., Robby T., T.: Hola: Zero-shot hoi detection with low-rank decomposed vlm feature adaptation. In: In Proceedings of the IEEE/CVF international conference on computer vision (2025)
22. Lei, Q., Wang, B., Tan, R.: Ez-hoi: Vlm adaptation via guided prompt learning for zero-shot hoi detection. *Advances in Neural Information Processing Systems* **37**, 55831–55857 (2024)
23. Lei, Q., Wang, B., Tan, R.T.: Crosshoi-bench: A unified benchmark for hoi evaluation across vision-language models and hoi-specific methods. In: Proceedings of the IEEE/CVF Conference on Computer Vision and Pattern Recognition (CVPR) (2026)
24. Li, G., Jampani, V., Sun, D., Sevilla-Lara, L.: Locate: Localize and transfer object parts for weakly supervised affordance grounding. In: Proceedings of the IEEE/CVF Conference on Computer Vision and Pattern Recognition. pp. 10922–10931 (2023)
25. Liu, J., Li, T., Cao, X., Ma, Y., Shang, G., Huang, H., Zhang, C., Chang, X., Huang, Z., Hu, J., et al.: Tele-omni: a unified multimodal framework for video generation and editing. arXiv preprint arXiv:2602.09609 (2026)
26. Liu, S., Zeng, Z., Ren, T., Li, F., Zhang, H., Yang, J., Jiang, Q., Li, C., Yang, J., Su, H., et al.: Grounding dino: Marrying dino with grounded pre-training for open-set object detection. In: European conference on computer vision. pp. 38–55. Springer (2024)
27. Lu, P., Bansal, H., Xia, T., Liu, J., Li, C., Hajishirzi, H., Cheng, H., Chang, K.W., Galley, M., Gao, J.: Mathvista: Evaluating mathematical reasoning of foundation models in visual contexts. arXiv preprint arXiv:2310.02255 (2023)
28. Lüddecke, T., Ecker, A.: Image segmentation using text and image prompts. In: Proceedings of the IEEE/CVF conference on computer vision and pattern recognition. pp. 7086–7096 (2022)
29. Luo, H., Zhai, W., Zhang, J., Cao, Y., Tao, D.: Learning affordance grounding from exocentric images. In: Proceedings of the IEEE/CVF conference on computer vision and pattern recognition. pp. 2252–2261 (2022)
30. Ma, K., Dong, H., Mu, Y.: Local occupancy-enhanced object grasping with multiple triplanar projection. In: European Conference on Computer Vision. pp. 1–18. Springer (2024)
31. Mai, J., Yang, M., Luo, W.: Erasing integrated learning: A simple yet effective approach for weakly supervised object localization. In: CVPR. pp. 8766–8775 (2020)
32. Michel, P., Levy, O., Neubig, G.: Are sixteen heads really better than one? *Advances in neural information processing systems* **32** (2019)

33. Moon, W., Seong, H.S., Heo, J.P.: Selective contrastive learning for weakly supervised affordance grounding. In: Proceedings of the IEEE/CVF International Conference on Computer Vision. pp. 5210–5220 (2025)
34. Mur-Labadia, L., Guerrero, J.J., Martinez-Cantin, R.: Multi-label affordance mapping from egocentric vision. In: Proceedings of the IEEE/CVF International Conference on Computer Vision. pp. 5238–5249 (2023)
35. Myers, A., Kanazawa, A., Fermuller, C., Aloimonos, Y.: Affordance of object parts from geometric features. In: International Conference on Robotics and Automation2. pp. 5–6 (2015)
36. Pan, X., Gao, Y., Lin, Z., Tang, F., Dong, W., Yuan, H., Huang, F., Xu, C.: Unveiling the potential of structure preserving for weakly supervised object localization. In: Proceedings of the IEEE/CVF conference on computer vision and pattern recognition. pp. 11642–11651 (2021)
37. Radford, A., Kim, J.W., Hallacy, C., Ramesh, A., Goh, G., Agarwal, S., Sastry, G., Askell, A., Mishkin, P., Clark, J., et al.: Learning transferable visual models from natural language supervision. In: International conference on machine learning. pp. 8748–8763. PmLR (2021)
38. Sawatzky, J., Srikantha, A., Gall, J.: Weakly supervised affordance detection. In: Proceedings of the IEEE Conference on Computer Vision and Pattern Recognition. pp. 2795–2804 (2017)
39. Sun, P., Chen, S., Zhu, C., Xiao, F., Luo, P., Xie, S., Yan, Z.: Going denser with open-vocabulary part segmentation. In: Proceedings of the IEEE/CVF International Conference on Computer Vision. pp. 15453–15465 (2023)
40. Tang, J., Wei, Z., Zheng, G., Yang, S.: Closed-loop transfer for weakly-supervised affordance grounding. In: Proceedings of the IEEE/CVF International Conference on Computer Vision. pp. 9530–9539 (2025)
41. Wu, J., Kang, W., Tang, H., Hong, Y., Yan, Y.: On the faithfulness of vision transformer explanations. In: Proceedings of the IEEE/CVF Conference on Computer Vision and Pattern Recognition. pp. 10936–10945 (2024)
42. Wu, Z., Chen, X., Pan, Z., Liu, X., Liu, W., Dai, D., Gao, H., Ma, Y., Wu, C., Wang, B., et al.: Deepseek-vl2: Mixture-of-experts vision-language models for advanced multimodal understanding. arXiv preprint arXiv:2412.10302 (2024)
43. Xu, L., Gao, Y., Song, W., Hao, A.: Weakly supervised multimodal affordance grounding for egocentric images. In: Proceedings of the AAAI Conference on Artificial Intelligence. vol. 38, pp. 6324–6332 (2024)
44. Xu, P., Mu, Y.: Weakly-supervised affordance grounding guided by part-level semantic priors. arXiv preprint arXiv:2505.24103 (2025)
45. Yang, Y., Zhai, W., Luo, H., Cao, Y., Luo, J., Zha, Z.J.: Grounding 3d object affordance from 2d interactions in images. In: Proceedings of the IEEE/CVF International Conference on Computer Vision. pp. 10905–10915 (2023)
46. Yue, X., Ni, Y., Zhang, K., Zheng, T., Liu, R., Zhang, G., Stevens, S., Jiang, D., Ren, W., Sun, Y., et al.: Mmmu: A massive multi-discipline multimodal understanding and reasoning benchmark for expert agi. In: Proceedings of the IEEE/CVF conference on computer vision and pattern recognition. pp. 9556–9567 (2024)
47. Zhang, J., Khayatkhoei, M., Chhikara, P., Ilievski, F.: Mllms know where to look: Training-free perception of small visual details with multimodal llms. arXiv preprint arXiv:2502.17422 (2025)
48. Zhou, B., Khosla, A., Lapedriza, A., Oliva, A., Torralba, A.: Learning deep features for discriminative localization. In: Proceedings of the IEEE conference on computer vision and pattern recognition. pp. 2921–2929 (2016)

49. Zhu, J., Wang, W., Chen, Z., Liu, Z., Ye, S., Gu, L., Tian, H., Duan, Y., Su, W., Shao, J., et al.: Internvl3: Exploring advanced training and test-time recipes for open-source multimodal models. arXiv preprint arXiv:2504.10479 (2025)

Supplementary Material for Token-Based Affordance Grounding with Large Vision-Language Models

A Implementation Details

In this section, we provide additional implementation details of the proposed tokAG, our zero-shot affordance grounding framework. Specifically, we elaborate on the LVLM inference settings, the object-masking pipeline, and the mathematical formulations for our token-centric attention extraction and post-processing techniques.

A.1 LVLM Configuration and Inference Settings

We employ Qwen3-VL [3] (2B and 32B) as our LVLM (Large Vision Language Model) backbones. To facilitate the extraction of internal cross-attention maps, the models are instantiated with an eager attention implementation (i.e., `attn_implementation="eager"`), and we perform inference using `bfloat16` precision. The input images are processed by Qwen’s vision encoder, which maps the image into a spatial vision grid. To utilize implicit semantic signals in LVLMs, we prompt the model with the following template:

“When people perform {action} with {object_name}, which part of the {object_name} is used for ‘{action}’? Answer in one sentence.”

To constrain the predicted affordance regions within the target object, we employ CLIPSeg [28] as an off-the-shelf segmenter. By providing the target object’s name as a text prompt, the generated raw output logits are passed through a sigmoid activation function to obtain continuous probability maps. These maps are resized using interpolation and thresholded to form the binary object mask M_{obj} .

As formulated in Sec. 3.1 (main paper), during the LVLM generation, we extract the cross-attention maps corresponding to the generated text tokens. Based on the CLIPSeg-generated mask M_{obj} , we select the Top-1 token t^* that yields the highest spatial activation within the target object area (M_{obj}). The aggregated attention map of this selected token serves as the raw affordance heatmap. Initially at the LVLM’s vision grid resolution ($H_{grid} \times W_{grid}$), this heatmap is finally bilinearly upsampled to match the fixed input image size of 1000×1000 .

A.2 Attention Map Post-Processing

Although the selected attention map \mathcal{H} is constrained within the target object boundaries, the raw activations can sometimes be overly concentrated or exhibit peaks. This concentration is often further amplified by the ‘‘attention sink’’ phenomenon [17], where a few specific visual patches disproportionately absorb attention weights, thereby suppressing other semantically relevant regions. To mitigate this effect and ensure that the high-response regions adequately cover the entire functional parts, we apply a spatial refinement step as follows.

First, the upsampled and masked heatmap \mathcal{H} is normalized by its maximum value. We then apply a fractional power scaling of 0.75 to the heatmap:

$$\mathcal{H}_{scaled} = \mathcal{H}^{0.75}$$

This fractional scaling ($p < 1$) effectively softens overly sparse and highly concentrated attention patches, amplifying weak but relevant interaction cues to form a more cohesive functional region.

Finally, to ensure spatial continuity and soften rigid boundaries, we apply an adaptive Gaussian blur. Since the final heatmap must be overlaid onto the original image for affordance visualization, we maintain scale invariance by dynamically calculating the standard deviation σ and the kernel size K based on the original image dimensions ($W_{orig} \times H_{orig}$), rather than the fixed 1000×1000 resolution used during LVLM inference:

$$\sigma = \min(W_{orig}, H_{orig}) \times 0.05$$

$$K = 2 \times \lfloor 3\sigma \rfloor + 1$$

Following the blurring operation, the heatmap undergoes a final min-max normalization to yield the ultimate affordance probability distribution, ranging strictly between 0 and 1.

B Additional Ablation Studies

B.1 Effect of Input Prompt Design

In our framework, the LVLM’s internal cross-attention map is conditioned on the generated textual response, which is driven by the input prompt. To evaluate the robustness of our token-centric attention extraction mechanism under different instructions, we conducted an ablation study using 11 different prompts. As detailed in Table S1, we varied both the system instructions (ranging from a standard ‘‘helpful assistant’’ to an ‘‘analytical computer vision model’’) and the specific phrasing of the user query.

The quantitative results demonstrate the stability of our approach. Despite variations in the linguistic structure and tone of the input prompts, the affordance grounding performance remains comparable across different instructions. Assigning an analytical role to the LVLM, such as ‘‘an AI vision analyzer’’ (Case

1) or “a task-oriented visual AI” (Case 2), leads to slight performance improvements (e.g., KLD of 1.039 for Case 1). However, the “Original” prompt, which specifies the action-object relationship without strict formatting constraints, also achieves competitive results. We therefore use it as the default configuration in the main experiments to demonstrate that the proposed framework works well without relying on extensive prompt engineering.

Table S1: Ablation study on the effect of different input prompt designs on the AGD20K dataset (Set 2). We vary the system instructions and user queries to evaluate the robustness of our affordance grounding framework. Cases 1–3 include a single-sentence length constraint, whereas Cases 4–10 remove this constraint. The best performance is **bolded** and the second-best is underlined.

ID	System Prompt	User Prompt	KLD ↓	SIM ↑	NSS ↑
Original	You are a helpful language and vision assistant.	When people perform {action} with {object_name}, which part of the {object_name} is used for ‘{action}’? answer in one sentence.	1.060	0.455	1.514
Case_1	You are an AI vision analyzer.	Identify the exact part of the {object_name} that people use to ‘{action}’. Keep your response to one sentence.	1.039	<u>0.461</u>	1.532
Case_2	You are a task-oriented visual AI.	Your task is to identify the part of the {object_name} used for ‘{action}’. Provide the answer in one sentence.	<u>1.057</u>	0.461	1.509
Case_3	You are a simple and clear AI assistant.	To ‘{action}’, what part of the {object_name} do you need? Give me a one-sentence answer.	1.067	0.451	<u>1.522</u>
Case_4	You are an AI vision analyzer.	Identify the exact part of the {object_name} that people use to ‘{action}’.	1.107	0.452	1.453
Case_5	You are a task-oriented visual AI.	Your task is to identify the part of the {object_name} used for ‘{action}’.	1.102	0.455	1.472
Case_6	You are a simple and clear AI assistant.	To ‘{action}’, what part of the {object_name} do you need?	1.125	0.439	1.437
Case_7	You are a spatial-aware vision assistant.	Locate and describe the specific physical area on the {object_name} where the ‘{action}’ takes place.	1.082	0.456	1.472

Continued on next page...

Table S1 – continued from previous page

ID	System Prompt	User Prompt	KLD ↓	SIM ↑	NSS ↑
Case_8	You are an action-recognition specialist.	are Focusing on the action ‘{action}’, detail the exact component of the {object_name} that affords this interaction.	1.162	0.437	1.383
Case_9	You are a direct and helpful assistant.	What is the primary part of the {object_name} that is required to ‘{action}’?	1.087	0.449	1.481
Case_10	You are an analytical AI that understands object affordances.	Analyze the relationship between the action ‘{action}’ and the {object_name}. Which part of the object is manipulated or interacted with?	1.129	0.438	1.440

In addition, we investigate the impact of output length constraints on attention quality. When comparing Cases 1–3 against their unconstrained counterparts (Cases 4–6), a performance difference is observed. For instance, Case 1 incorporates the directive, “Keep your response to one sentence,” whereas Case 4 uses the same instruction (“Identify the exact part of the {object_name} that people use to ‘{action}’.”) but omits the length constraint. As shown in Table S1, the unconstrained prompts show lower performance across the metrics (e.g., a KLD of 1.107 for Case 4 versus 1.039 for Case 1). We attribute this to the tendency of LVLMs to generate longer, descriptive responses when unconstrained at inference time. This added length introduces linguistic noise, diluting the cross-modal attention weights across task-irrelevant words and background visual patches. By applying a single-sentence limit, the model is guided to produce a concise and semantically focused response. Consequently this length constraint helps suppress background noise and allows the model’s internal cross-attention to focus on the target affordance region, yielding improved spatial grounding.

Beyond optimizing individual prompts through such constraints, we also note the possibility of a multi-prompt ensemble strategy [16]. By aggregating the cross-attention maps generated from multiple distinct prompts for a single image–action pair, it may be possible to further stabilize the predictions and achieve additional performance gains. However, while effective as an engineering technique, this ensemble approach requires executing the LVLm inference multiple times per sample, which linearly increases the computational cost and inference latency. Because the core focus of our work lies in the zero-shot token-centric attention extraction framework itself, and a single generic prompt already achieves competitive performance efficiently, we do not include the multi-prompt ensemble. We discuss it here as a possible extension for scenarios where accuracy is prioritized over computational efficiency.

B.2 Effect of Layer and Head Selection

In the main paper, Table 5 presents an ablation study comparing our proposed aggregation method against specific layer and head selection strategies (Methods A and B). The rationale for isolating particular combinations, such as Layer 25 Head 5 (L25-H5) and Layer 16 Head 15 (L16-H15), is inspired by recent findings from Kang *et al.* [18],

which suggest that large vision-language models only require a select few attention heads for image segmentation tasks.

To systematically identify these optimal heads within our framework, we extracted the internal cross-attention maps from all individual layers and heads during the LVLM generation process. We then computed a spatial similarity score by comparing each head’s attention map against the explicit object mask generated by CLIPSeg. The specific layer-head combinations (e.g., L25-H5 and L16-H15) were chosen because they yielded the maximum similarity scores, indicating that these selected heads focus on the target object within the image.

However, as discussed in the main paper, relying on a single optimal layer or head is often insufficient for precise affordance grounding. Through our analysis of the cross-modal attention maps between generated output tokens and visual patches, two key observations emerge: first, spatial activations across different layers and heads are very diverse, often focusing on different image regions; second, individual attention responses can be diffuse. Despite this variance, we observe that the activations falling within the target object boundary tend to correlate with the specific functional parts associated with the queried action (e.g., highlighting the mattress for the action “sit on bed”). Because these attention maps originate from action-conditioned output tokens generated by the LVLM, they contain rich and diverse functional cues. Therefore, our proposed approach (Method C, Table 5 main paper), which aggregates attention across all layers and heads, effectively synthesizes this diverse distribution. As demonstrated in Table 5 in the main paper, this comprehensive aggregation helps mitigate diffuse background noise and captures the nuanced semantic consensus required to pinpoint zero-shot affordance regions, outperforming single-head or single-layer selections.

To further substantiate the necessity of our aggregation approach, we conducted an experiment evaluating all possible partial aggregation strategies. Specifically, as detailed in Table S2, we investigated the performance of layer-wise aggregation (averaging attention maps across all heads within each individual layer) and head-wise aggregation (averaging across all layers for each individual head). While certain partial aggregations may occasionally show competitive metrics, they generally fall short of the robust spatial grounding achieved by comprehensively aggregating across both dimensions. We acknowledge that exhaustively searching for and optimizing a highly specific subset of layers and heads could theoretically yield marginal performance gains. However, the optimal configuration is sensitive to the specific LVLM architecture and the given image distribution. More importantly, determining such an optimal subset requires task-specific ground-truth annotations or validation sets to guide the selection process. Relying on such data-driven heuristic engineering contradicts the premise of our zero-shot setting. Therefore, our aggregation across all layers and heads serves as a robust, model-agnostic strategy, eliminating the need for manual tuning while maintaining the zero-shot nature of our framework.

Table S2: Comprehensive performance comparison of various partial aggregation strategies on the AGD20K dataset (Set 2). The table reports the results of aggregating all heads within each layer (Layer-wise) and aggregating all layers for each head (Head-wise). Within each category (Layer-wise, Head-wise, and Ours), the best performance is **bolded** and the second-best is underlined.

Aggregation Strategy Configuration	KLD ↓	SIM ↑	NSS ↑
Layer-wise (Aggregating All Heads)			
Layer 1	1.303	0.388	1.175
Layer 2	1.389	0.369	1.060
Layer 3	1.288	0.404	1.207
Layer 4	1.266	0.397	1.204
Layer 5	1.245	0.409	1.251
Layer 6	1.335	0.390	1.124
Layer 7	1.172	0.442	1.354
Layer 8	1.248	0.406	1.227
Layer 9	1.218	0.412	1.278
Layer 10	1.163	0.428	1.349
Layer 11	1.300	0.401	1.150
Layer 12	1.080	0.424	1.489
Layer 13	1.121	0.439	1.413
Layer 14	1.105	0.459	1.459
Layer 15	1.100	0.456	1.459
Layer 16	1.060	0.454	1.508
Layer 17	1.100	0.461	1.466
Layer 18	1.109	0.456	1.446
Layer 19	1.087	0.447	1.466
Layer 20	<u>1.065</u>	0.453	1.514
Layer 21	1.070	0.449	1.502
Layer 22	1.067	0.445	<u>1.511</u>
Layer 23	1.066	0.451	1.495
Layer 24	1.070	<u>0.460</u>	1.492
Layer 25	1.066	0.447	1.498
Layer 26	1.089	0.450	1.471
Layer 27	1.093	0.447	1.464
Layer 28	1.318	0.390	1.152
Head-wise (Aggregating All Layers)			
Head 1	1.142	0.429	1.388
Head 2	1.099	0.445	1.445

Continued on next page...

Table S2 – continued from previous page

Aggregation Strategy Configuration		KLD ↓	SIM ↑	NSS ↑
	Head 3	1.086	0.455	1.483
	Head 4	1.104	0.442	1.462
	Head 5	<u>1.061</u>	0.454	<u>1.507</u>
	Head 6	1.063	0.454	1.513
	Head 7	1.077	0.455	1.469
	Head 8	1.105	0.438	1.437
	Head 9	1.078	0.442	1.500
	Head 10	1.101	0.443	1.447
	Head 11	1.143	0.430	1.403
	Head 12	1.070	0.459	1.506
	Head 13	1.063	0.458	1.499
	Head 14	1.079	<u>0.461</u>	1.505
	Head 15	1.061	0.465	1.501
	Head 16	1.100	0.450	1.476
Ours – Method C	All Layers & Heads	1.060	0.455	1.514

C Additional Quantitative Results

C.1 Generalization to Different LVLN Backbones

In the main paper, we demonstrated the zero-shot affordance grounding capabilities of our framework primarily utilizing the Qwen3-VL [3] backbone. To investigate whether our token-centric attention extraction mechanism generalizes across different Large Vision-Language Models (LVLNs), we conducted an additional experiment where we replace the backbone with InternVL3 [49] (2B parameters).

As shown in Table S3, while Qwen3-VL (2B) achieves slightly better performance, our framework with InternVL3 (2B) still surpasses previous state-of-the-art weakly supervised methods, demonstrating good generalization across different LVLN backbones. Specifically, on AGD20K-Set 2 (Unseen), our method with InternVL3 (2B) achieves a KLD of 1.183 and an SIM of 0.429, outperforming recent baselines such as LoopTrans (KLD 1.247) and Moon et al. (KLD 1.243). This indicates that our zero-shot approach is not strictly tied to a specific architecture and can leverage the implicit semantic signals of different LVLNs.

C.2 Comparison with WSAG-PLSP

While our main quantitative evaluation in Table 2 (main paper) focuses on comparable weakly supervised baselines in the zero-shot setting, we provide an additional comparison with the recently proposed WSAG-PLSP [44] in Table S4. WSAG-PLSP introduces a paradigm that leverages Large Language Models (LLMs) to generate target texts, followed by a refinement process guided by ground-truth knowledge available in the AGD20K dataset. This access to dataset-specific priors during the training or refinement phase helps the model obtain more accurate textual and spatial alignment.

Table S3: Performance comparison on the AGD20K-Set 2 (Unseen) dataset using different LVLM backbones. The best performance is **bolded** and the second-best is underlined.

Method	AGD20K-Set 2 (Unseen)		
	KLD ↓	SIM ↑	NSS ↑
Cross-View-AG+ [29]	1.765	0.279	0.882
LOCATE [24]	1.405	0.372	1.157
INTRA [15]	1.365	0.375	1.209
WSMA [43]	1.335	0.382	1.220
LoopTrans [40]	1.247	0.403	1.315
Moon et al. [33]	1.243	0.405	<u>1.368</u>
Ours – InternVL3(2B)	<u>1.183</u>	<u>0.429</u>	1.323
Ours – Qwen3-VL(2B)	1.060	0.455	1.514

Table S4: Performance comparison on AGD20K-Set 1 and Set 2. Best results are **bolded** and second-best results are underlined.

Method	AGD20K-Set 1			AGD20K-Set 2		
	KLD↓	SIM↑	NSS↑	KLD↓	SIM↑	NSS↑
WSAG-PLSP (ICLR’25) [44]	0.890	0.510	1.547	1.153	0.437	1.418
Ours (2B)	1.020	<u>0.459</u>	1.406	<u>1.060</u>	0.455	<u>1.514</u>
Ours (32B)	<u>1.010</u>	0.458	<u>1.424</u>	1.043	0.455	1.549

Notably, WSAG-PLSP relies on dataset-specific refinement during training, whereas our method operates in a fully zero-shot manner.

As shown in Table S4, this strategy is advantageous on the AGD20K-Set 1 (Seen) split, where WSAG-PLSP benefits from learning the target area distribution and therefore achieves higher performance. However, we observe that on the AGD20K-Set 2 (Unseen) split, our zero-shot framework demonstrates generalization, outperforming WSAG-PLSP across the evaluated metrics (e.g., a KLD of 1.043 vs. 1.153) without requiring task-specific data-driven refinement.

Given these methodological differences, quantitative metrics alone may not fully reflect the qualitative nuances and utility of the grounded affordances. To provide a broader evaluation, we conducted a blind user study on AGD20K-Set 1 to compare the quality and human alignment of the affordance regions predicted by WSAG-PLSP and our proposed method, as detailed in D.

D User Study

D.1 User Study Comparison with WSAG-PLSP

Study Setup To further evaluate the perceptual quality of the predicted affordance heatmaps, we conducted a user study comparing TokAG with three existing methods: LOCATE [24], WSMA [43], and WSAG-PLSP [44].

We randomly sample 170 images from the AGD20K test set. For each image, we present the predicted affordance heatmaps produced by the four methods. The predictions from the four methods are displayed in random order and anonymized as Method 1–4 to ensure a blind comparison and avoid potential bias toward any specific method.

Participants are asked to select the predictions that best match the expected interaction for the given action–object pair. Multiple selections are allowed when several predictions are judged to equally capture this expected interaction. Furthermore, an option to select “None” is provided in cases where no prediction adequately reflects the expected interaction.

Annotation Procedure Each participant evaluated the full set of 170 images independently. For each image, participants selected one or more predictions that best match the expected interaction for the given action–object pair. The annotations were recorded using a structured JSON format, where each entry corresponds to one image and stores the selected method indices. An example annotation entry is shown below:

```
{
  "image_id": "push_motorcycle_000123",
  "selected_methods": [2,4]
}
```

This format allows multiple selections when several predictions are judged to equally match the expected interaction for the given action–object pair.

Preference Rate Let N denote the number of sampled images and A denote the number of annotators. For annotator a , let $S_i^{(a)}$ denote the set of methods selected for image i , where multiple selections are allowed if several predictions are judged equally capture the expected interaction for the given action–object pair. The selection rate of method m for annotator a is defined as

$$P_m^{(a)} = \frac{1}{N} \sum_{i=1}^N \mathbf{1}(m \in S_i^{(a)}), \quad (4)$$

where $\mathbf{1}(m \in S_i^{(a)})$ equals 1 if method m is selected for image i , and 0 otherwise. We report the average preference rate across annotators:

$$\bar{P}_m = \frac{1}{A} \sum_{a=1}^A P_m^{(a)}. \quad (5)$$

This metric measures the proportion of images for which a method is judged by annotators to be one of the predictions most consistent with the ground-truth affordance map. Because multiple selections are allowed, the preference rates of different methods do not necessarily sum to 100%.

Table S5 presents the quantitative results of the user study conducted on 170 sampled images. The selection rates indicate the frequency with which each method’s

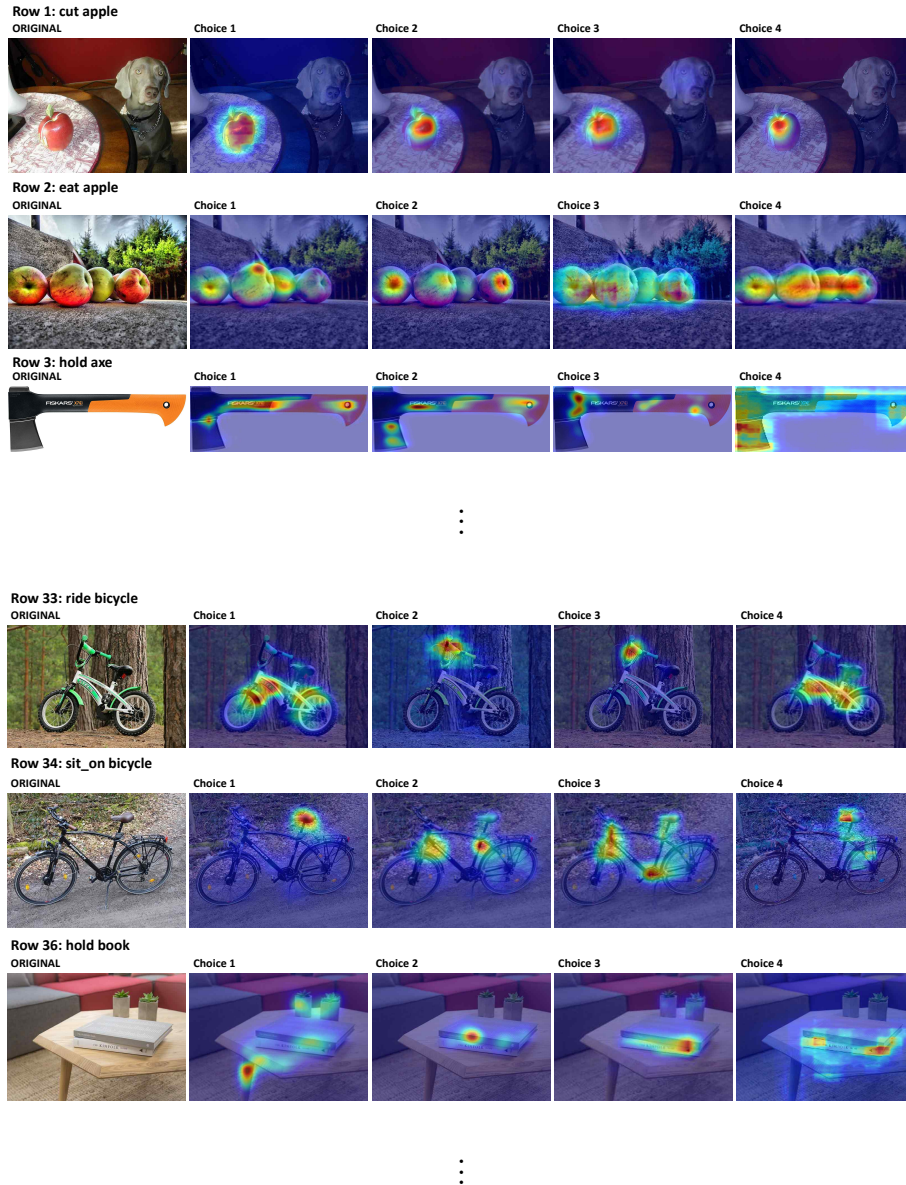


Fig. S1: Examples from the user study. For each row, the original input and the predicted affordance heatmaps from four methods were shown. The order of the methods was randomized and anonymized as Choice 1–4 during the annotation process. Participants were asked to select the prediction(s) that best match the expected interaction for the given action–object pair.

Table S5: User study results on 170 randomly sampled AGD20K test images. We report the preference rate (%) for each method, where a higher value indicates that the method is more frequently judged to best match the expected interaction for the given action–object pair.

Method	Annotator 1	Annotator 2	Average
LOCATE	57.6	24.1	40.9
WSMA	54.7	21.8	38.3
WSAG-PLSP	56.5	25.3	40.9
TokAG	70.6	35.9	53.3

prediction was judged by the annotators to be the closest to the expected interaction. We include several example pages of the annotation interface as shown in Figure S1. The full set of annotated images contains 170 samples used for the user study.

Across the evaluations from both annotators, our proposed TokAG records the highest average selection rate of 53.3%. Specifically, TokAG was selected in 70.6% and 35.9% of the cases by Annotator 1 and Annotator 2, respectively. In comparison, the baseline methods yielded lower average rates: WSAG-PLSP and LOCATE both recorded 40.9%, while WSMA recorded 38.3%.

We observe a variance in the absolute selection rates between the two annotators. This difference reflects the inherent subjectivity of affordance evaluation and varying degrees of annotator leniency regarding multiple selections. However, despite this variance in absolute values, the relative performance trend among the evaluated methods remains consistent across both annotators. Overall, these quantitative outcomes indicate that the spatial heatmaps generated by our TokAG are more frequently evaluated by human annotators as best reflecting the expected interaction for the given action–object pair.

E Additional Qualitative Results

E.1 Additional Visual Comparisons

As illustrated in Figure S2 and Figure S3, we provide additional visualization results across various action–object categories. Across the evaluated categories, TokAG tends to produce more localized affordance predictions compared to existing approaches such as LOCATE [24], WSMA [43], and WSAG-PLSP [44].

For instance, in action categories such as *hold* and *sit on*, our approach localizes the predicted heatmaps specifically to the expected interaction areas (e.g., handles and saddles). In contrast, the baseline methods often produce heatmaps that are more dispersed or mapped to non-interactive regions of the objects. These additional examples further show that TokAG generates affordance regions that align well with expected human interactions.

E.2 Examples of Generated Sentences

As described in our methodology, TokAG isolates target affordance regions through an output token selection mechanism based on the sentences generated by the LVLM

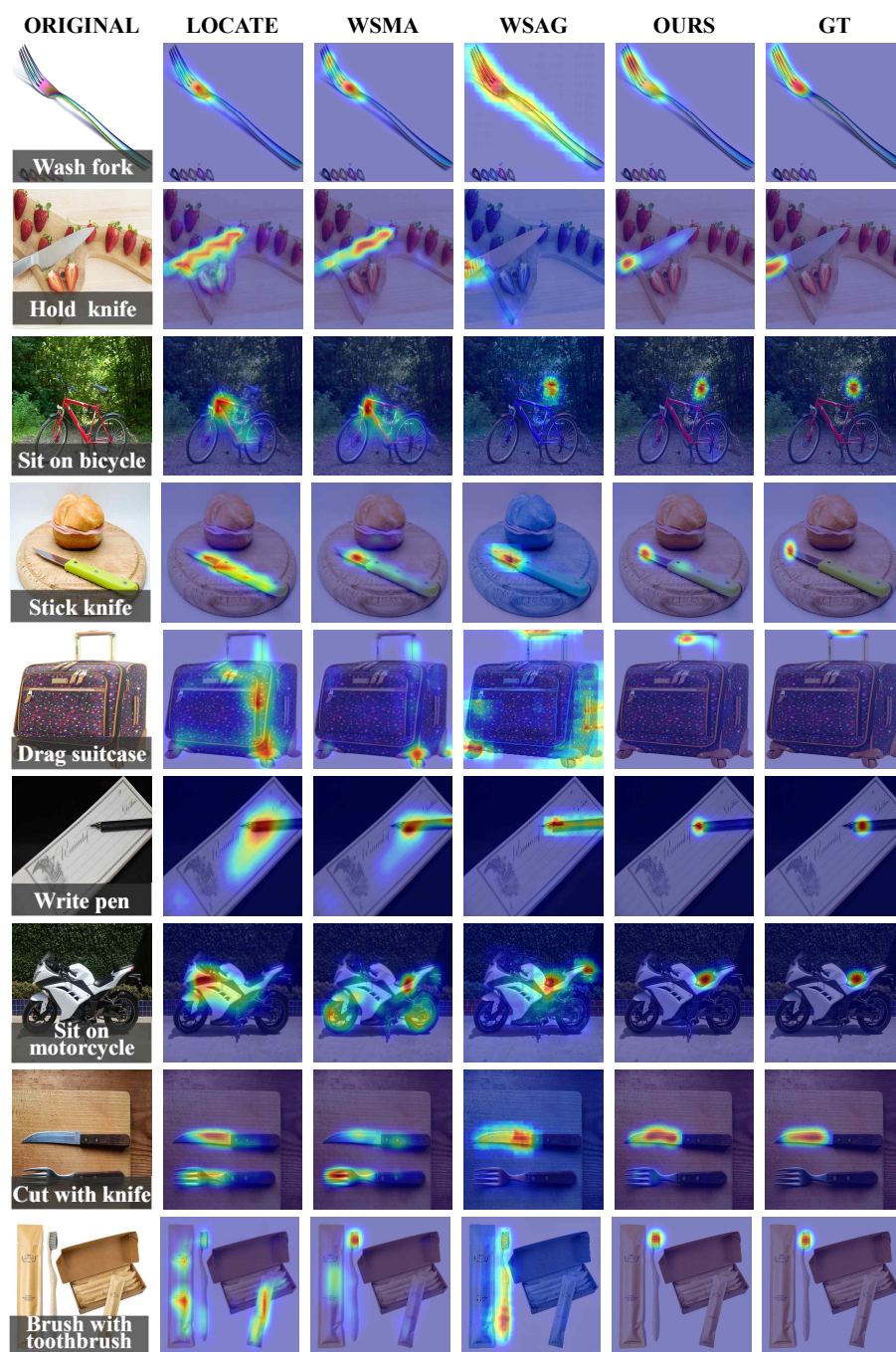


Fig. S2: Qualitative comparison of affordance grounding results. We show predictions of TokAG (ours) together with LOCATE [24], WSMA [43], WSAG-PLSP [44], and the ground truth (GT).

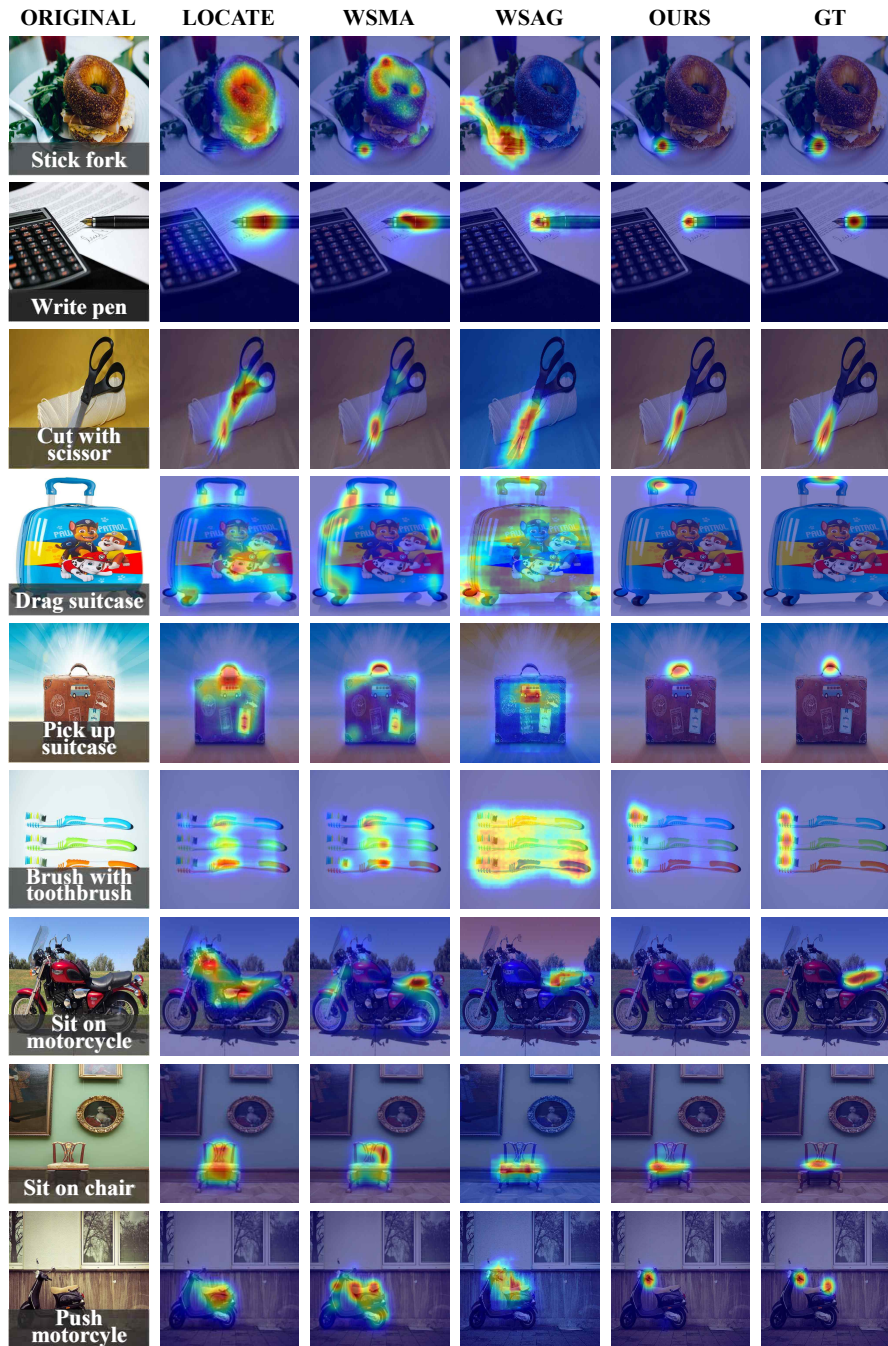


Fig. S3: Qualitative comparison of affordance grounding results. We show predictions of TokAG (ours) together with LOCATE [24], WSMA [43], WSAG-PLSP [44], and the ground truth (GT).

(Large Vision-Language Model). To provide a clearer understanding of this process, Table S6 shows examples of the generated sentences together with the selected top tokens used for cross-attention extraction. These examples illustrate how the LVLMM describes the functional parts associated with different action-object pairs and the selected token used to localize the affordance region in our method.

Table S6: Examples of generated sentences for different action-object pairs. Given only the action and object categories, the LVLMM generates a sentence describing the functional part involved in the interaction. The column “Top Token” shows the token selected by our token selection mechanism from the generated sentence.

Action	Object	Top Token	Generated Response
<i>carry</i>	<i>skis</i>	base	The part of the skis used for ‘carry’ is the base, which is the bottom surface of the ski that is in contact with the snow.
<i>catch</i>	<i>soccer ball</i>	surface	The part of the soccer ball used for ‘catch’ is the surface that is in contact with the player’s hand or glove, typically the top of the ball.
<i>cut</i>	<i>banana</i>	peel	The peel is used for cutting a banana.
<i>cut_with</i>	<i>knife</i>	blade	The blade of the knife is used for ‘cut with’.
<i>drink_with</i>	<i>cup</i>	's	The part of the cup used for ‘drink with’ is the cup’s handle.
<i>eat</i>	<i>banana</i>	yellow	The part of the banana used for eating is the flesh, which is the yellow, sweet, and edible part of the fruit.
<i>eat</i>	<i>broccoli</i>	ret	The floret of the broccoli is used for eating.
<i>hit</i>	<i>axe</i>	metal	The part of the axe used for ‘hit’ is the head, which is the metal part at the end of the axe.
<i>hold</i>	<i>axe</i>	The	The handle of the axe is used for holding.
<i>hold</i>	<i>cup</i>	handle	The handle of the cup is used for ‘hold’.
<i>hold</i>	<i>golf clubs</i>	grip	The part of the golf club used for ‘hold’ is the grip.
<i>hold</i>	<i>knife</i>	handle	The handle of the knife is used for ‘hold’.
<i>hold</i>	<i>skis</i>	base	The part of the skis used for ‘hold’ is the base, which is the bottom surface of the ski.
<i>jump</i>	<i>skis</i>	base	The part of the skis used for ‘jump’ is the base, which is the bottom surface of the ski that provides the lift and propulsion for the jump.
<i>kick</i>	<i>soccer ball</i>	ball	The part of the soccer ball used for ‘kick’ is the bottom.
<i>lie_on</i>	<i>bed</i>	mattress	The part of the bed used for ‘lie on’ is the mattress.
<i>open</i>	<i>refrigerator</i>	top	The top part of the refrigerator is used for ‘open’.
<i>peel</i>	<i>banana</i>	outer	The peel of the banana is the outer skin that is removed, typically from the stem end to the tip.
<i>pick_up</i>	<i>skis</i>	base	The part of the skis used for ‘pick up’ is the base, which is the bottom surface of the ski.
<i>pour</i>	<i>cup</i>	sp	The part of the cup used for pouring is the spout.
<i>push</i>	<i>bicycle</i>	the	The part of the bicycle used for ‘push’ is the pedal.

Continued on next page...

Table S6 – continued from previous page

Action	Object	Top Token	Generated Response
<i>ride</i>	<i>bicycle</i>	frame	The part of the bicycle used for ‘ride’ is the frame, which is the main structure that supports the rider and the wheels.
<i>sip</i>	<i>cup</i>	rim	The part of the cup used for ‘sip’ is the rim.
<i>sit_on</i>	<i>bed</i>	head	The headboard is used for ‘sit on’ with the bed.
<i>sit_on</i>	<i>bicycle</i>	seat	The seat of the bicycle is used for ‘sit on’.
<i>stick</i>	<i>knife</i>	handle	The handle of the knife is used for ‘stick’.
<i>swing</i>	<i>golf clubs</i>	head	The part of the golf club used for ‘swing’ is the club head.
<i>take_photo</i>	<i>camera</i>	lens	The lens is used for ‘take photo’ with the camera.
<i>throw</i>	<i>basketball</i>	surface	The part of the basketball used for ‘throw’ is the ball itself, specifically the surface that is in contact with the hand or arm during the throwing motion.
<i>type_on</i>	<i>laptop</i>	keyboard	The keyboard is the part of the laptop used for ‘type on’.
<i>wash</i>	<i>cup</i>	the	The part of the cup used for ‘wash’ is the inner surface of the cup, specifically the inside of the cup, which is cleaned with a wash cloth or sponge.
<i>wash</i>	<i>knife</i>	blade	The blade is used for washing.

E.3 Quantitative and Qualitative Results on an Additional Dataset: EPIC-Aff

To further evaluate the proposed TokAG, we conduct additional experiment on the EPIC-Aff dataset [34], a benchmark derived from the first-person perspective video dataset EPIC-Kitchens [10]. To match the scale of the AGD20K test set (540 images), we randomly sampled 500 images from the unseen split condition of EPIC-Aff. As summarized in Table S7, TokAG shows improved results compared to existing SOTA methods. In addition, we observe that the numbers of different evaluation metrics for all models on EPIC-Aff are lower than those on AGD20K; this discrepancy may come from the dataset characteristics of EPIC-Aff, which contains fewer object-centric ground-truth regions. Despite these characteristics, TokAG isolates the target affordance areas, as shown in Figure S4. TokAG localizes the functional regions, indicating that the proposed token-based grounding framework transfers to different domain distributions without further fine-tuning.

Table S7: Quantitative comparison on the EPIC-Aff dataset.

Method	KLD ↓	SIM ↑	NSS ↑
LOCATE	3.901	0.071	0.366
WSMA	3.372	0.062	0.413
TokAG (Ours)	3.367	0.122	0.927

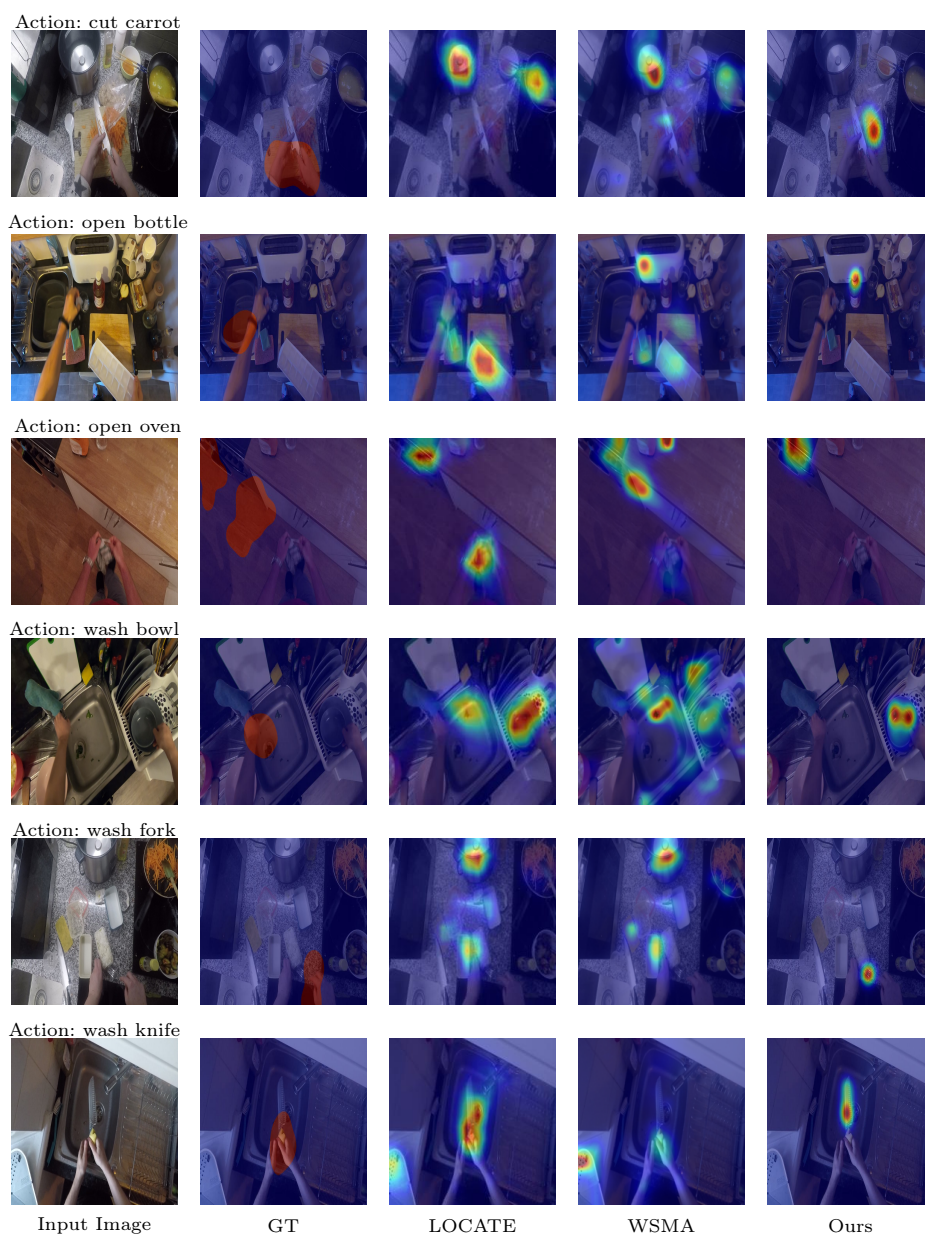


Fig. S4: Qualitative comparison on the EPIC-Aff dataset.